Historic Yangtze flooding of 2020 tied to extreme Indian Ocean conditions

Zhen-Qiang Zhou (周震强)[a,b,c], Shang-Ping Xie (谢尚平)[d,1], and Renhe Zhang (张人禾)[a,b,c,1]

[a]Department of Atmospheric and Oceanic Sciences and Institute of Atmospheric Sciences, Fudan University, Shanghai 200438, China; [b]CMA-FDU Joint Laboratory of Marine Meteorology, Shanghai 200438, China; [c]Innovation Center of Ocean and Atmosphere System, Zhuhai Fudan Innovation Research Institute, Zhuhai 518057, China; and [d]Scripps Institution of Oceanography, University of California San Diego, La Jolla, CA 92093

Edited by John M. Wallace, University of Washington, Seattle, WA, and approved January 26, 2021 (received for review October 24, 2020)

Heavy monsoon rainfall ravaged a large swath of East Asia in summer 2020. Severe flooding of the Yangtze River displaced millions of residents in the midst of a historic public health crisis. This extreme rainy season was not anticipated from El Niño conditions. Using observations and model experiments, we show that the record strong Indian Ocean Dipole event in 2019 is an important contributor to the extreme Yangtze flooding of 2020. This Indian Ocean mode and a weak El Niño in the Pacific excite downwelling oceanic Rossby waves that propagate slowly westward south of the equator. At a mooring in the Southwest Indian Ocean, the thermocline deepens by a record 70 m in late 2019. The deepened thermocline helps sustain the Indian Ocean warming through the 2020 summer. The Indian Ocean warming forces an anomalous anticyclone in the lower troposphere over the Indo-Northwest Pacific region and intensifies the upper-level westerly jet over East Asia, leading to heavy summer rainfall in the Yangtze Basin. These coupled ocean-atmosphere processes beyond the equatorial Pacific provide predictability. Indeed, dynamic models initialized with observed ocean state predicted the heavy summer rainfall in the Yangtze Basin as early as April 2020.

East Asia flooding | anomalous anticyclone | Indian Ocean | El Niño

Summer is the rainy season for East Asia. A northeastward-slanted rain band—called Mei-yu in China and Baiu in Japan—extends from the Yangtze River valley of China to the east of Japan during early summer (early June to mid-July). The Yangtze is the longest river of Asia, flowing from the eastern Tibetan Plateau and exiting into the ocean in Shanghai. Approximately one-third of the population of China live in the river basin. The Mei-yu rain band displays marked interannual variability with great socioeconomic impacts on the densely populated region, including agriculture production, water availability, food security, and economies (1–5).

During June through July 2020, the Mei-yu rain band intensified markedly, with rainfall exceeding the 1981 to 2010 mean of ~300 mm by ~300 mm over the Yangtze River valley (Fig. 1*A*). This corresponds to an excess of up to 4 SDs (Fig. 1*B*). By 12 July 2020, the Yangtze floods caused 141 deaths, 28,000 homes were flattened, and 3.53 million hectares of crops were affected, with the direct economic loss at 82.23 billion yuan (11.76 billion US dollars) (6). South of the Mei-yu rain band, negative rainfall anomalies (−60 mm/month) extended over a broad region from the Bay of Bengal to tropical Northwest Pacific (Fig. 1*A*). This meridional dipole of rainfall anomalies is known as the recurrent Pacific–Japan pattern (7).

In June through July 2020, an anomalous anticyclone with depressed rainfall dominates the lower troposphere over the tropical and subtropical Northwest Pacific through the South China Sea (Fig. 1*A*). The easterly wind anomalies on the south flank of the anomalous anticyclone extend into the North Indian Ocean, while the anomalous southwesterlies on the northwest flank transport water vapor from the south to feed the enhanced Mei-yu rainband (Fig. 1*C*). In the mid-troposphere, the westerlies intensify over midlatitude East Asia, and the anomalous mid-tropospheric warm advection from Tibet (Fig. 1*D*) adiabatically induce upward motions (Fig. 1*C*) to enhance Mei-yu rainfall. The resultant anomalous diabatic heating reinforces the anomalous vertical motion, forming a positive feedback (8–12). This is consistent with the empirical relationship known to Chinese forecasters between the 500 hPa geopotential height and the Mei-yu rain band.

On the interannual timescale, El Niño-Southern Oscillation (ENSO) has been identified as the dominant forcing of Mei-yu rainfall variability (3–5, 13). Mei-yu rainfall in the Yangtze Basin tends to increase (decrease) in post-El Niño (La Niña) summer. A Northwest Pacific anomalous anticyclone often develops rapidly during an El Niño winter (14), interacting with local sea surface temperature (SST) (15, 16) and modulated by the background annual cycle (17). The anomalous anticyclone cools the tropical Northwest Pacific on the southeastern flank by strengthening the northeast trade winds and surface evaporation. The ocean cooling suppresses atmospheric convection, reinforcing the anomalous anticyclone with a Rossby wave response. El Niño also causes the tropical Indian Ocean to warm. The Indo-western Pacific Ocean capacitor refers to the following interbasin positive feedback in summer between the Indian Ocean warming and the Northwest Pacific anomalous anticyclone. The tropical Indian Ocean warming excites a Matsuno-Gill-type (18, 19) response in tropospheric temperature, with a Kelvin response that penetrates eastward and induces northeasterly surface wind anomalies in the tropical Northwest Pacific. The resultant Ekman divergence suppresses convection and induces the anomalous anticyclone (20). The anomalous anticyclone in turn feeds back to

Significance

Summer rainfall along the Yangtze River in 2020 was the heaviest since 1961, with devastating socioeconomic impacts. While official forecasts based on tropical Pacific state failed, we show that dynamic models, when initialized with ocean observations globally, succeed in predicting the extreme rainfall. Slowly propagating oceanic Rossby waves in the South Indian Ocean are the source of predictability, which are in turn tied to the record-breaking Indian Ocean Dipole in late 2019. The identification of antecedent subsurface conditions of the Indian Ocean as a key predictor represents an important conceptual advance in Asian summer monsoon dynamics, helping improve disaster preparation that saves lives and properties.

Author contributions: Z.-Q.Z., S.-P.X., and R.Z. designed research; Z.-Q.Z., S.-P.X., and R.Z. performed research; Z.-Q.Z. analyzed data; and Z.-Q.Z., S.-P.X., and R.Z. wrote the paper.

The authors declare no competing interest.

This article is a PNAS Direct Submission.

[1]To whom correspondence may be addressed. Email: sxie@ucsd.edu or rhzhang@fudan.edu.cn.

This article contains supporting information online at https://www.pnas.org/lookup/suppl/doi:10.1073/pnas.2022255118/-/DCSupplemental.

Published March 8, 2021.

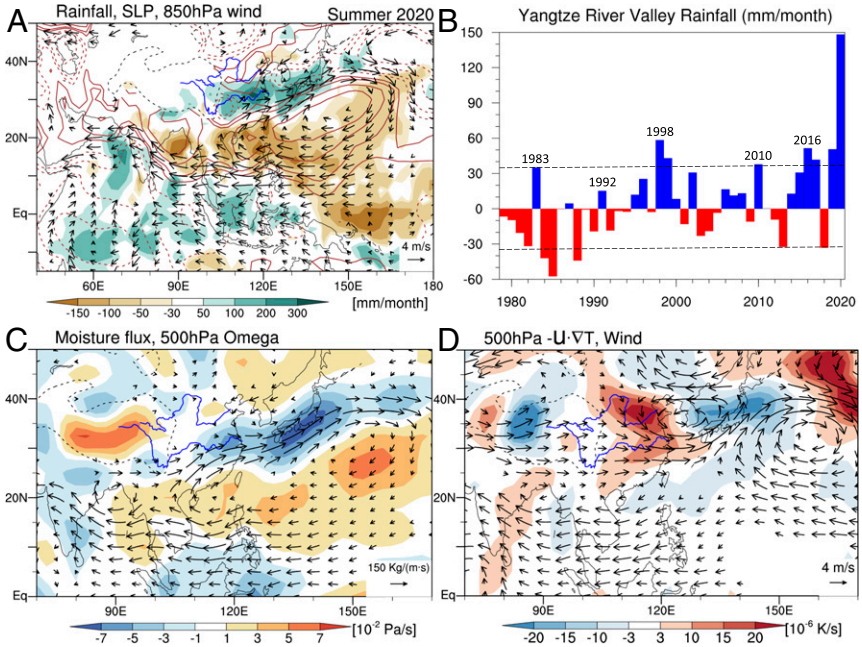

Fig. 1. Atmospheric dynamics of the Yangtze flooding of 2020. June through July averaged anomalies of (*A*) rainfall (shading, mm/month), SLP (contours at ±0.3, ±0.6, ±1.2, and ±1.8 hPa), and 850 hPa wind (vector, displayed with speed > 0.3 m/s); (*C*) column-integrated moisture transport (vector, displayed with magnitude > 15 kg · m^{-1} · s^{-1}) and 500 hPa omega (shading, Pa/s, and negative values for ascent motions); and (*D*) 500 hPa horizontal temperature advection (shading, K/s) and wind (vector, displayed with speed > 0.5 m/s). Blue solid curves denote the Yangtze and Yellow Rivers. Black dashed curves (2,000 m isoline of topography) denote the Tibetan Plateau and surrounding mountains. SLP anomalies over and north of Tibetan Plateau are masked out for clarity. (*B*) June through July averaged rainfall anomalies (mm/month) over the Yangtze River Valley (26° to 33°N, 105° to 122°E) during 1979 to 2020, with one SD of 35 mm/month. Major El Niño events are marked.

the North Indian Ocean warming by weakening the background southwest monsoon and suppressing surface evaporation (21–23).

The above ocean-atmospheric coupling processes work well for major El Niño events and provide predictability for Mei-yu rainfall over East Asia (Fig. 1*B*). A robust Northwest Pacific anomalous anticyclone developed during the summers of 1998 and 2016, each following a major El Niño. A strong anomalous anticyclone and excessive Mei-yu rainfall were not expected for 2020 summer, however, since in the 2019/20 winter (November to January), the Niño3.4 index was marginal at only 0.5 °C (*SI Appendix*, Fig. S1) as compared to 2.4 °C and 2.6 °C in 1997/98 and 2015/16 winters, respectively. SST anomalies in the equatorial central Pacific (Niño4) were positive and nearly constant in magnitude during May 2018 to May 2020 (*SI Appendix*, Fig. S1), but the Northwest Pacific anomalous anticyclone did not develop in 2019 summer. Then what caused the pronounced anomalous anticyclone during the 2020 summer? Was it due to unpredictable atmospheric internal dynamics as in August 2016 (24, 25), or did some predictable SST anomalies play a role?

Atmospheric Model Experiments

To evaluate the SST effect, we force the state-of-the-art Community Atmosphere Model version 6 (CAM6) with observed monthly SST anomalies (Fig. 2*A*) (see *Materials and Methods* for details). Forced with global SST anomalies (referred to as GLOBAL, Fig. 2*B*), the atmospheric model simulates both the excessive Mei-yu rainfall and low-level anomalous anticyclone over the Northwest Pacific during June 2020, although the anomalous easterlies are too weak over the Bay of Bengal through the South China Sea compared to observations. Mei-yu rainfall anomalies over the Yangtze Basin are over 90 mm/month (Fig. 2*B*), comparable with observations (Fig. 1*A*). This indicates that the excessive Mei-yu rainfall and anomalous anticyclone of June 2020 are largely forced by SST anomalies instead of due to internal atmospheric dynamics.

The SST anomalies are positive over the tropical Indian Ocean and a weak La Niña developed over the tropical Pacific in June 2020 (Fig. 2*A*). To evaluate relative importance of Pacific and Indian Ocean SST anomalies, we conduct another two experiments forced separately by tropical Pacific (referred to as PACIFIC) and Indian Ocean (referred to as INDIAN) SST anomalies. In June 2020, the tropical Indian Ocean is anomalously warm (Fig. 2*A*). The INDIAN run largely reproduces the results of the GLOBAL run, including positive Mei-yu rainfall anomalies over the Yangtze Basin and negative rainfall anomalies to the south with the anomalous anticyclone (Fig. 2*D*). In comparison, tropical Pacific anomalies only play a limited role (Fig. 2*E*). The weak and eastward-displaced anomalous anticyclone south of Japan in the PACIFIC experiment seems forced by depressed rainfall in the equatorial central Pacific as a Rossby wave response (Fig. 2*E*), due to the rapid transition from El Niño to La Niña in early summer of 2020 (*SI Appendix*, Fig. S1).

Over the Southwest Indian Ocean, positive SST anomalies induce deep convection with an anomalous cyclonic circulation as well as the northeasterlies (northwesterlies) north (south) of the equator (Fig. 2 *B* and *D*). Over the North Indian Ocean, the anomalous northeasterlies induce positive SST anomalies by weakening the climatological monsoon westerlies to reduce surface evaporation. The GLOBAL run successfully reproduces the enhanced mid-tropospheric westerly jet in the midlatitudes, which induces adiabatic ascending motion by advecting warm temperature from the Tibetan Plateau through the Yangtze Basin to the North Pacific (Fig. 2*C*). The adiabatic ascent, together with increased moisture transport by the low-level anomalous anticyclone, sets up a favorable condition for the excessive Mei-yu rainfall. The GLOBAL run does not reproduce all the midlatitude anomalies, including wavy perturbations along the westerly

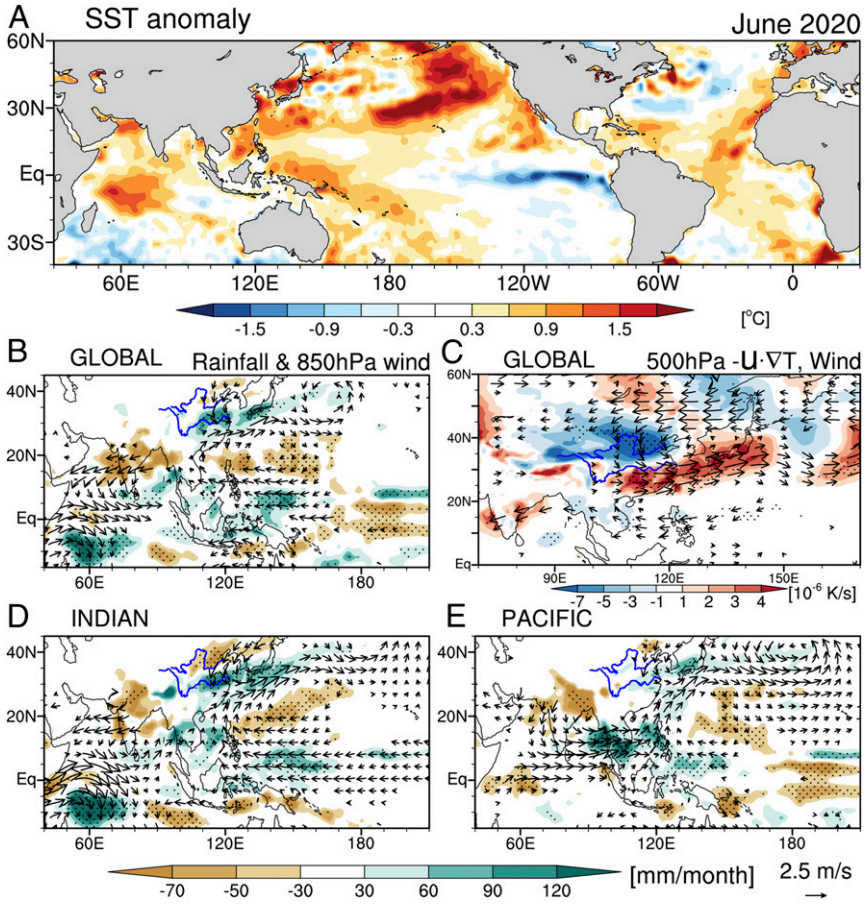

Fig. 2. SST forcing effects. (*A*) SST anomalies in June 2020. Rainfall (shading, mm/month) and 850 hPa wind (vector, displayed with speed > 0.3 m/s) anomalies in June 2020 from three atmospheric model simulations forced by global SST (GLOBAL) (*B*), tropical Indian Ocean SST (INDIAN) (*D*), and tropical Pacific SST (PACIFIC) (*E*). (*C*) Same as *B* but for 500 hPa wind (vector, displayed with speed > 0.5 m/s) and horizontal temperature advection (shading, K/s). See *Materials and Methods* for details. The stippling denotes where the ensemble mean exceeds 0.6 SD of the ensemble spread.

jet in observations (Fig. 1*D*) known as the Silk Road Pattern (26–28), because of atmospheric internal dynamics unrelated to SST variability. The model results indicate that the excessive Mei-yu rainfall and anomalous anticyclone of 2020 are largely due to tropical Indian Ocean SST anomalies, with some contribution from the tropical Pacific.

Indian Ocean Processes

The next question is what caused the Indian Ocean warming? A major Indian Ocean Dipole (IOD) took place in 2019, with the dipole mode index peaking at 2.1 °C in October (Fig. 3*A* and *SI Appendix*, Fig. S1), the highest on record (29, 30). The weak 2019/20 El Niño event probably contributed but by itself cannot explain the record-breaking IOD event of 2019. Over the eastern Indian Ocean, strong easterly/southeasterly wind anomalies (5 m/s) occurred along the equator and the Java–Sumatra coasts during September through November 2019 (Fig. 3*A*). The equatorial easterly wind anomalies shoal the thermocline, bring cold water to the surface, and amplify the SST cooling along the Java–Sumatra coasts. The ocean cooling strengthens the zonal SST gradient and the easterly/southeasterly winds on the equator/Indonesian coast. This is known as Bjerknes feedback, originally proposed for El Niño growth. The anomalous anticyclonic wind curls associated with the equatorial easterlies force downwelling oceanic Rossby waves that slowly propagate westward south of the equator (Fig. 3*B*) (31, 32). The downwelling oceanic Rossby waves deepen the thermocline in the South Indian Ocean (Fig. 3*B*), accompanied by copropagating positive SST anomalies (*SI Appendix*, Fig. S5*A*). In September through November 2019, the deepened thermocline causes the sea surface to rise anomalously in the Southwest Indian Ocean centered at 8°S, 75°E (Fig. 3*A*). At a mooring at 8°S, 67°E, the 20 °C isotherm (a proxy of the thermocline) is shallow at 80 m on average but took a deep dive to 150 m in November 2019 (Fig. 3*C*), a record of the 14-y deployment (*SI Appendix*, Fig. S4). The slow-propagating oceanic Rossby waves allow the Southwest Indian Ocean warming to persist through the 2020 summer (*SI Appendix*, Figs. S1 and S5*A*). The Southwest Indian Ocean warming intensifies local convection and induces northerly wind anomalies across the equator during 2020 spring to early summer (*SI Appendix*, Fig. S5 *A* and *B*). The Coriolis effect creates an easterly component north and westerly component south of the equator. Over the North Indian Ocean, the anomalous northeasterlies weaken the climatological monsoon westerlies in 2020 summer, reducing surface evaporation and increasing SST (Fig. 2). Indeed, the Indian Ocean warming and the anomalous anticyclone over the Northwest Pacific are coupled with positive feedback known as the Indo-western Pacific Ocean capacitor (Fig. 1 and *SI Appendix*, Fig. S7*A*). Both the low-level anomalous anticyclone and enhanced upper-level westerly jet contribute to the heavy rainfall along the Yangtze River.

The anomalous anticyclonic wind curls over the South Indian Ocean begin in 2019 summer and last through the following spring (Fig. 3*B*). The atmospheric model experiments indicate that the

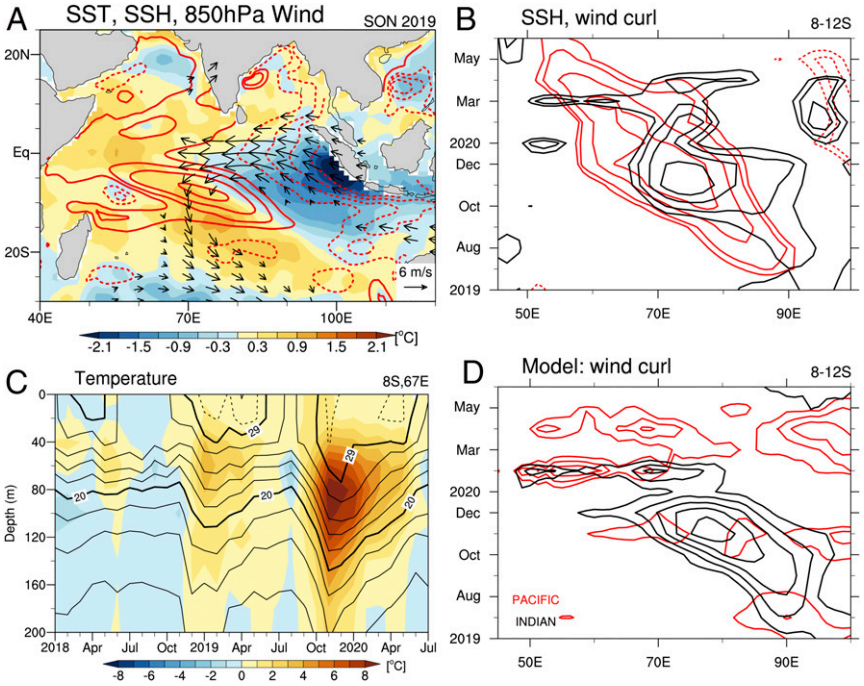

Fig. 3. Indian Ocean anomalies. (*A*) SST (shading, °C), sea surface height (SSH, red contour, ±5, ±10, ±15, and ±20 cm), and 850 hPa wind (vector, displayed with speed > 1.5 m/s) anomalies during September through November 2019. (*B*) Longitude-time diagram of SSH (red contour, ±8, ±10, ±15, and ±20 cm) and 10 m wind stress curl (black contour, 0.25, 0.4, 0.6, 0.8, and 10^{-5} N · m^{-3}) anomalies averaged over 8° to 12°S during June 2019 to June 2020. (*C*) Time-depth section of ocean temperature (contour, from 14 °C to 28 °C with interval of 2 °C; thick black lines for 20 °C and 29 °C; dashed lines for 29.5 °C) and the anomalies (shading, °C) at a mooring in the Southwest Indian Ocean (8°S, 67°E) during January 2018 to July 2020. (*D*) The 1,000 hPa wind stress curl anomalies averaged over 8° to 12°S during June 2019 to June 2020 for INDIAN (black contour, 0.2, 0.3, 0.4, 0.5, 0.6, and 10^{-5} N · m^{-3}) and PACIFIC (red contour, 0.1, 0.15, 0.2, and 10^{-5} N · m^{-3}) runs. Wind curls are downward positive in *B* and *D*.

IOD event causes the anticyclone wind curls through December 2019, while Pacific SST anomalies, notably the warming in the equatorial western Pacific as part of the weak El Niño (*SI Appendix*, Fig. S5*C*), contribute to the sustained wind curls thereafter in early 2020 and hence to the record thermocline deepening in the South Indian Ocean (Fig. 3*D*).

The above coupled ocean-atmospheric processes imply predictability at monthly and longer leads, as oceanic Rossby waves carry the memory of wind forcing in the past and propagate slowly westward. Fig. 4 shows the rainfall anomalies in June 2020 predicted by the North American Multi-Model Ensemble (NMME) (*Materials and Methods*) at various time leads. The coupled ocean-atmosphere models in NMME allow for skillful forecasts at lead times of one to several months. The multi-model ensemble averages show that the forecasts initialized on 1 June 2020 predict heavy rainfall (above 90 mm/month) over the Yangtze Basin and an anomalous anticyclone over the Northwest Pacific in June 2020 (Fig. 4*D*), consistent with observations (Fig. 4*E*). An independent study reports a similar success of the Japan Meteorological Agency dynamic forecast system in capturing enhanced Meiyu-Baiu rainfall in 2020 (33). As early as April 2020, the NMME predicts the meridional dipole between rainfall decrease over the tropical Northwest Pacific and intensified Mei-yu (Fig. 4*C*), while the decreased rainfall in the anomalous anticyclone over the Northwest Pacific shows up in the ensemble mean as early as February 2020 (Fig. 4*B*). Increased SST and convective rainfall over the Southwest Indian Ocean occur when the models are initialized in November 2019 with observed subsurface ocean temperatures that include downwelling oceanic Rossby waves (Fig. 4 and *SI Appendix*, Fig. S6). The successful multi-model ensemble forecasts confirm that the Yangtze flooding of 2020 was due to coupled ocean-atmospheric processes, anchored by oceanic Rossby waves in the South Indian Ocean.

Discussion

Our observational analysis and model experiments show that the historic Yangtze flooding in 2020 summer is due to the combined effect of the record strong IOD and weak central Pacific El Niño in late 2019. Fig. 5 is a schematic of the oceanic and atmospheric processes involved. In fall 2019, a record-breaking IOD, coupled with the easterly wind anomalies through the Bjerknes feedback, developed in the tropical Indian Ocean. By weakening the Walker circulation, a weak El Niño contributed to, but was probably not the deciding factor for, the extreme 2019 IOD event. Historically, ENSO is but one mechanism that triggers IOD (34, 35); a major IOD event took place in 1961 without El Niño. The anticyclonic wind curls associated with the strong IOD and weak El Niño forced downwelling oceanic Rossby waves that slowly propagated westward (Figs. 5*A* and 3*B*). The Rossby waves caused the Southwest Indian Ocean to warm as the deepened thermocline increased the temperature of the water upwelled into the surface mixed layer (Figs. 5*B* and 3*B* and *SI Appendix*, Fig. S5*A*). The persistent Southwest Indian Ocean warming induced an asymmetrical pattern of anomalous atmospheric circulation over the tropical Indian Ocean during 2020 spring to early summer, with the northeasterlies (northwesterlies) north (south) of the equator (Figs. 5*B* and 2 and *SI Appendix*, Fig. S5*B*). Over the North Indian Ocean and the South China Sea, the anomalous northeasterlies weakened the climatological monsoon southwesterlies during May to June 2020, reducing surface evaporation and increasing SST (Fig. 5*B*). The Indian Ocean warming in summer 2020 induced the low-level anomalous anticyclone over the Northwest Pacific and intensified the upper-level westerly jet over the Yangtze Basin. The intensified moisture transport by the anomalous anticyclone, together with the anomalous ascending motions induced by the enhanced westerly jet, caused heavy rainfall along the Yangtze River (Fig. 5*B*).

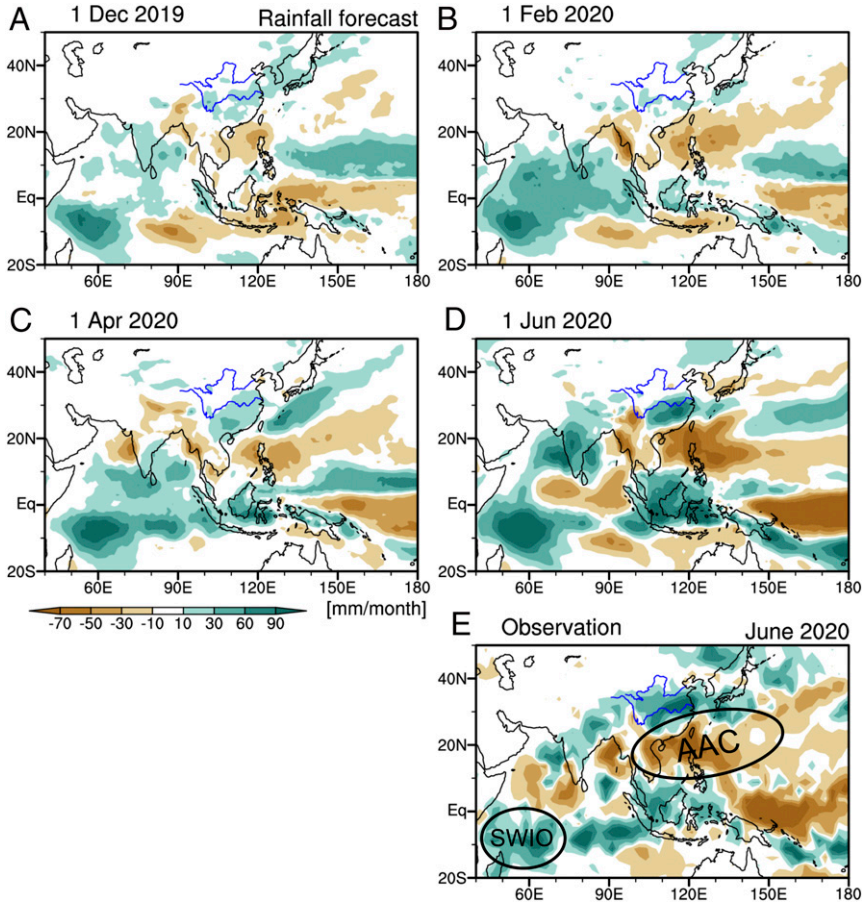

Fig. 4. Multi-model ensemble seasonal forecasts. Multi-model ensemble average anomalies of rainfall (shading, mm/month) in June 2020 at various time leads (*A*–*D*; the initialization dates are marked at the top left of each panel) and in observations (*E*, scaled by a factor of 0.5 for easy comparison). Black circles in *E* denote the key factors of interest: the Southwest Indian Ocean (SWIO) deep convection and Northwest Pacific anomalous anticyclone (AAC).

The official forecasts did not anticipate the extreme Mei-yu rainfall in 2020 summer, but we showed that initialized coupled models successfully predicted the anomalous anticyclone and excessive Mei-yu rainfall over East Asia. In retrospect, the successful multi-model ensemble forecasts would have allowed a lead time of 1 to 3 months in advance for local authorities to implement preventive measures and reduce the loss of lives and properties (Fig. 4 and *SI Appendix*, Fig. S6). Our study suggests that the successful dynamic prediction is enabled by oceanic Rossby waves in the South Indian Ocean, which are in turn induced by the strong IOD event of 2019 and weak El Niño condition in the western Pacific. The IOD mode of Bjerknes feedback (36) and Indo-western Pacific Ocean capacitor (20) represent major advances in Indian Ocean climate dynamics over the recent decades. While this framework emphasizes ENSO forcing, our results show that other non-ENSO factors are important not only for the IOD but also the Indo-western Pacific Ocean capacitor and, by extension, monsoon rainfall over East Asia. Further research to better understand, model, and observe these factors (e.g., oceanic Rossby waves in the South Indian Ocean) holds the promise of improving seasonal predictions of the East Asia summer monsoon.

In a warming climate, the frequency of extreme IOD and El Niño occurrences increases in most climate models (37, 38). Increased extreme IOD occurrences have profound socioeconomic impacts on the densely populated Asian monsoon region both directly (36, 37) and indirectly, as illustrated in the Yangtze flooding of 2020.

Materials and Methods

Observational Data. We use monthly precipitation from the Climate Prediction Center Merged Analysis of Precipitation (CMAP) (39); monthly air temperature, zonal and meridional winds, vertical velocity, specific humidity, and sea level pressure (SLP) from the National Centers for Environmental Prediction–National Center for Atmospheric Research (NCEP–NCAR) reanalysis dataset (40); and monthly sea surface height from the NCEP Global Ocean Data Assimilation System (41). Monthly regional SST indices are calculated using the National Oceanic and Atmospheric Administration Optimum Interpolation Sea Surface Temperature version 2 dataset (42), including the Niño 3.4 (5°S to 5°N and 170°W to 120°W), Niño 4 (5°S to 5°N and 160°E to 150°W), and IOD index (anomalous SST gradient between the western [50°E to 70°E and 10°S to 10°N] and southeastern [90°E to 110°E and 10°S to 0°N] equatorial Indian Ocean). The above datasets can be obtained from https://www.esrl.noaa.gov/psd/data/gridded. We focus on a 42-y period from 1979 to 2020 (limited by CMAP's satellite rainfall estimates). Monthly anomalies are derived relative to the climatological mean (1981 to 2010) after removing the linear trend over the whole period. Monthly ocean temperature data in Fig. 3*C* are from a buoy of the Research Moored Array for African–Asian–Australian Monsoon Analysis and Prediction (43) at 8°S, 67°E from 2007 to 2020, obtained from https://www.pmel.noaa.gov/tao/drupal/disdel.

AGCM Experiments. We use the CAM6 to investigate the role of SST forcing in the Yangtze flooding of 2020. CAM6 is the latest global atmosphere model of the NCAR and the atmospheric component of the Community Earth System Model (CESM) version 2.1.2. The model resolution is 0.9° latitude × 1.25° longitude ("f09_f09") with 30 sigma levels in the vertical. We performed four runs forced with the monthly SST climatology (CONTROL), the detrended monthly SST anomalies for January 2019 to July 2020 globally (GLOBAL), and regionally over the tropical Pacific Ocean (25°S to 25°N,

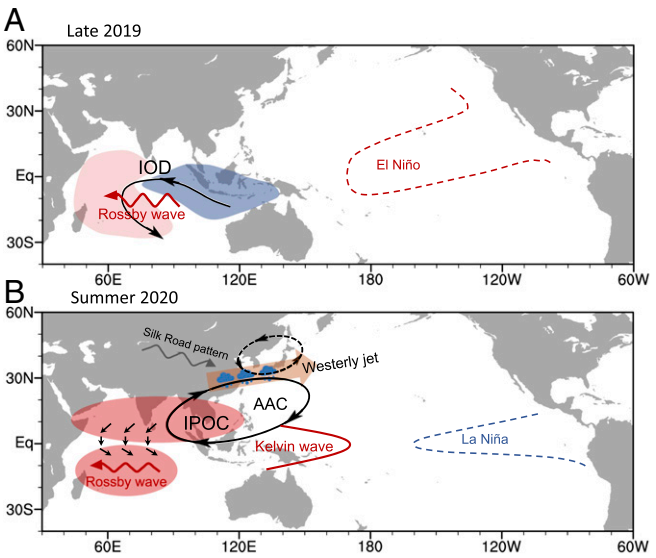

Fig. 5. Schematic for physical processes causing the 2020 Yangtze flooding. (*A*) The record strong IOD (shading) and weak El Niño excite westward oceanic Rossby waves in the South Indian Ocean in late 2019 and early 2020. (*B*) Rossby wave-induced Southwest Indian Ocean warming forces an anti-symmetrical wind pattern that is most pronounced in spring 2020. The resultant North Indian Ocean warming excites an anomalous anticyclone over the Indo-Northwest Pacific, contributing to the excessive rainfall along the Yangtze River in summer 2020.

120°E to 80°W, PACIFIC) and Indian Ocean (25°S to 25°N, 40° to 120°E, INDIAN). The CONTROL run has 30 members, and the other experiments have 20 members, each with slightly different initial conditions. The ensemble averages are analyzed. A caveat of imposing partial SST anomalies in limited domains is that it would induce artificial SST gradient and spurious convective response near the boundaries (120°E, in our case) (Fig. 2 *D* and *E*). With global SST forcing, the model captures salient atmospheric anomalies over the summer Indo-western Pacific, consistent with results from long historical simulations beyond the 2020 summer (21, 22, 25).

The model rainfall climatology is too low over the Mei-yu region and too high over the Indo–China Peninsula in June and July (*SI Appendix*, Fig. S2). In July, the midlatitude westerly jet is displaced about 10° northward compared to observations because of the early onset of deep convection over the tropical Northwest Pacific (44, 45). Regarding interannual variability, the model simulates the low-level anomalous anticyclone and intensifies upper-level westerlies in both June and July (Fig. 2 and *SI Appendix*, Fig. S3). It captures enhanced rainfall over the Mei-yu region in June (Fig. 2), but not in July of 2020 (*SI Appendix*, Fig. S3). Similar difficulty in simulating July Mei-yu rainfall variability is reported with the UK Meteorological Office seasonal forecast system (46).

Operational Seasonal Forecasts. We use the NMME prediction (47), based on coupled models in the United States and Canada (https://www.cpc.ncep.noaa.gov/products/NMME/).

Data Availability. AGCM experiments (netcdf) data have been deposited in GitHub (https://github.com/zhenqiangzhou/Yangzte).

ACKNOWLEDGMENTS. We thank three anonymous reviewers for constructive comments. Z.-Q.Z. and R.Z. were supported by the National Key R&D Program of China (2016YFA0600602) and the National Natural Science Foundation of China (41790472, 41805044), and S.-P.X. was supported by the NSF (AGS 1637450). The CESM project is supported primarily by the NSF. Model experiments were performed at the High-End Computing Center of Fudan University.

1. K. Ninomiya, T. Murakami, "The early summer rainy season (Baiu) over Japan" in *Monsoon Meteorology*, C. P. Chang, T. N. Krishnamurti, Eds. (Oxford University Press, New York, 1987), pp. 93–121.
2. C. Fu, X. Teng, The relationship between ENSO and climate anomaly in China during the summer time. *Sci. Atmos. Sin.* **12**, 133–141 (1988).
3. R. Huang, Y. Wu, The influence of ENSO on the summer climate change in China and its mechanism. *Adv. Atmos. Sci.* **6**, 21–32 (1989).
4. R. Huang, W. Chen, B. Yang, R. Zhang, Recent advances in studies of the interaction between the East Asian winter and summer monsoons and ENSO cycle. *Adv. Atmos. Sci.* **21**, 407–424 (2004).
5. Y. Ding, P. Liang, Y. Liu, Y. Zhang, Multiscale variability of Meiyu and its prediction: A new review. *J. Geophys. Res. Atmos.* **125**, e2019JD031496 (2020).
6. Huaxia, China raises flood response to second-highest level. *Xinhua News*, 12 July 2020. http://www.xinhuanet.com/english/2020-07/12/c_139207054.htm. Accessed 1 September 2020.
7. T. Nitta, Long-term variations of cloud amount in the Western Pacific region. *J. Meteorol. Soc. Jpn.* **64**, 373–390 (1986).
8. T. Sampe, S.-P. Xie, Large-scale dynamics of the meiyu-baiu rainband: Environmental forcing by the westerly jet. *J. Clim.* **23**, 113–134 (2010).
9. Y. Kosaka, S.-P. Xie, H. Nakamura, Dynamics of interannual variability in summer precipitation over East Asia. *J. Clim.* **24**, 5435–5453 (2011).
10. W. Kong, J. C. H. Chiang, Southward shift of Westerlies intensifies the East Asian early summer rainband following El Niño. *Geophys. Res. Lett.* **47**, 1–10 (2020).
11. R. Lu, Z. Lin, Role of subtropical precipitation anomalies in maintaining the summertime meridional teleconnection over the western North Pacific and East Asia. *J. Clim.* **22**, 2058–2072 (2009).
12. X. Sun, R. J. Greatbatch, W. Park, M. Latif, Two major modes of variability of the East Asian summer monsoon. *Q. J. R. Meteorol. Soc.* **136**, 829–841 (2010).
13. M. Tanaka, Interannual and interdecadal variations of the Western North Pacific monsoon and Baiu rainfall and their relationship to the ENSO cycles. *J. Meteorol. Soc. Jpn.* **75**, 1109–1123 (1997).
14. R. Zhang, A. Sumi, M. Kimoto, Impact of El Niño on the East Asian monsoon: A diagnostic study of the '86/87 and '91/92 events. *J. Meteorol. Soc. Jpn.* **74**, 49–62 (1996).
15. C. Wang, R. H. Weisberg, J. I. Virmani, Western Pacific interannual variability associated with the El Niño-Southern oscillation. *J. Geophys. Res. Oceans* **104**, 5131–5149 (1999).
16. B. Wang, R. Wu, X. Fu, Pacific-East Asian teleconnection: How does ENSO affect East Asian climate? *J. Clim.* **13**, 1517–1536 (2000).
17. M. F. Stuecker, A. Timmermann, F.-F. Jin, S. McGregor, H.-L. Ren, A combination mode of the annual cycle and the El Niño/Southern Oscillation. *Nat. Geosci.* **6**, 540–544 (2013).
18. T. Matsuno, Quasi-geostrophic motions in the Equatorial area. *J. Meteorol. Soc. Jpn.* **44**, 25–43 (1966).
19. A. E. Gill, Some simple solutions for heat-induced tropical circulation. *Q. J. R. Meteorol. Soc.* **106**, 447–462 (1980).
20. S.-P. Xie *et al.*, Indian Ocean capacitor effect on Indo–Western Pacific climate during the summer following El Niño. *J. Clim.* **22**, 730–747 (2009).
21. Y. Kosaka, S.-P. Xie, N.-C. Lau, G. A. Vecchi, Origin of seasonal predictability for summer climate over the Northwestern Pacific. *Proc. Natl. Acad. Sci. U.S.A.* **110**, 7574–7579 (2013).
22. Z.-Q. Zhou, S.-P. Xie, G. J. Zhang, W. Zhou, Evaluating AMIP skill in simulating interannual variability over the Indo-western Pacific. *J. Clim.* **31**, 2253–2265 (2018).
23. C.-Y. Wang, S.-P. Xie, Y. Kosaka, ENSO-unrelated variability in Indo–Northwest Pacific climate: Regional coupled Ocean–Atmospheric feedback. *J. Clim.* **33**, 4095–4108 (2020).
24. C. Li, W. Chen, X. Hong, R. Lu, Why was the strengthening of rainfall in summer over the Yangtze River valley in 2016 less pronounced than that in 1998 under similar preceding El Niño events?—Role of midlatitude circulation in August. *Adv. Atmos. Sci.* **34**, 1290–1300 (2017).
25. X. Wang, S.-P. Xie, Z. Guan, Atmospheric internal variability in the summer Indo–Northwestern Pacific: Role of the intraseasonal oscillation. *J. Clim.* **33**, 3395–3410 (2020).
26. R. Wu, A mid-latitude Asian circulation anomaly pattern in boreal summer and its connection with the Indian and East Asian summer monsoons. *Int. J. Climatol.* **22**, 1879–1895 (2002).
27. T. Enomoto, Interannual variability of the Bonin high associated with the propagation of Rossby waves along the Asian jet. *J. Meteorol. Soc. Jpn.* **82**, 1019–1034 (2004).
28. Q. Ding, B. Wang, Circumglobal teleconnection in the Northern Hemisphere summer. *J. Clim.* **18**, 3483–3505 (2005).
29. T. Doi, S. K. Behera, T. Yamagata, Predictability of the super IOD Event in 2019 and its link With El Niño modoki. *Geophys. Res. Lett.* **47**, 1–9 (2020).
30. Y. Du *et al.*, Thermocline warming induced extreme Indian Ocean Dipole in 2019. *Geophys. Res. Lett.* **47**, e2020GL090079 (2020).
31. S.-P. Xie, H. Annamalai, F. A. Schott, J. P. McCreary, Structure and mechanisms of South Indian Ocean climate variability. *J. Clim.* **15**, 864–878 (2002).
32. W. Yu, B. Xiang, L. Liu, N. Liu, Understanding the origins of interannual thermocline variations in the tropical Indian Ocean. *Geophys. Res. Lett.* **32**, 1–4 (2005).
33. Y. Takaya, I. Ishikawa, C. Kobayashi, H. Endo, T. Ose, Enhanced Meiyu-Baiu rainfall in early summer 2020: Aftermath of the 2019 super IOD event. *Geophys. Res. Lett.* **47**, e2020GL090671 (2020).
34. R. Zhang, Y. Tan, El Nino and interannual variation of the sea surface temperature in the tropical Indian Ocean. *Proc. SPIE–Int. Soc. Opt. Eng.* **4899**, 11–17 (2003).

35. Y. Yang *et al*., Seasonality and predictability of the Indian Ocean Dipole mode: ENSO forcing and internal variability. *J. Clim.* **28**, 8021–8036 (2015).
36. N. H. Saji, B. N. Goswami, P. N. Vinayachandran, T. Yamagata, A dipole mode in the tropical Indian Ocean. *Nature* **401**, 360–363 (1999).
37. W. Cai *et al*., Increased frequency of extreme Indian Ocean dipole events due to greenhouse warming. *Nature* **510**, 254–258 (2014).
38. W. Cai *et al*., Increasing frequency of extreme El Niño events due to greenhouse warming. *Nat. Clim. Chang.* **4**, 111–116 (2014).
39. P. Xie, P. A. Arkin, Analyses of global monthly precipitation using gauge observations, satellite estimates, and numerical model predictions. *J. Clim.* **9**, 840–858 (1996).
40. E. Kalnay *et al*., The NCEP/NCAR reanalysis project. *Bull. Am. Meteorol. Soc.* **77**, 437–472 (1995).
41. D. Behringer, Y. Xue, Evaluation of the global ocean data assimilation system at NCEP: The Pacific Ocean. https://ams.confex.com/ams/84Annual/webprogram/Paper70720.html. Accessed 1 September 2020.
42. R. W. Reynolds, N. A. Rayner, T. M. Smith, D. C. Stokes, W. Wang, An improved in situ and satellite SST analysis for climate. *J. Clim.* **15**, 1609–1625 (2002).
43. M. J. McPhaden *et al*., RAMA: The research moored array for African-Asian-Australian monsoon analysis and prediction. *Bull. Am. Meteorol. Soc.* **90**, 459–480 (2009).
44. H. Ueda, T. Yasunari, R. Kawamura, Abrupt seasonal change of large-scale convective activity over the western Pacific in the northern summer. *J. Meteorol. Soc. Jpn.* **73**, 795–809 (1995).
45. W. Zhou, S.-P. Xie, Z.-Q. Zhou, Slow preconditioning for the abrupt convective jump over the northwest Pacific during summer. *J. Clim.* **29**, 8103–8113 (2016).
46. G. M. Martin, N. J. Dunstone, A. A. Scaife, P. E. Bett, Predicting June mean rainfall in the middle/lower Yangtze River basin. *Adv. Atmos. Sci.* **37**, 29–41 (2020).
47. B. P. Kirtman *et al*., The North American multimodel ensemble: Phase-1 seasonal-to-interannual prediction; phase-2 toward developing intraseasonal prediction. *Bull. Am. Meteorol. Soc.* **95**, 585–601 (2014).